NASA CR-777

THE FLUTTER OF FLEXIBLE, TOWED TENSION SHELLS

By Richard H. MacNeal

Prepared under Contract ~~No.~~ NAS 1-5605 by
ASTRO RESEARCH CORP~~ORATION~~
Santa Barbara, Calif.

for Langley Research Center

NATIONAL AERONAUTICS AND SPACE ADMINISTRATION

For sale by the Clearinghouse for Federal Scientific and Technical Information
Springfield, Virginia 22151 – CFSTI price $3.00

CONTENTS

	Page
SUMMARY	1
INTRODUCTION	1
SYMBOLS	2
DESCRIPTION OF THE PROBLEM	4
METHOD OF ANALYSIS	6
RESULTS OF NUMERICAL CALCULATION	12
CONCLUDING DISCUSSION	15
APPENDIX A Aerodynamic Force Coefficients	16
APPENDIX B Energy Expressions	20
APPENDIX C Formulas for Elements in the Module Representing a Section of Membrane Shell	29
REFERENCES	34
TABLE	35
FIGURES	36

THE FLUTTER OF FLEXIBLE, TOWED TENSION SHELLS

By Richard H. MacNeal
Astro Research Corporation

SUMMARY

A method of aeroelastic analysis for axisymmetric membrane shells is developed and is applied to the flutter of a flared tension cone decelerator attached by a cable to a massive forebody. The principal result is that the presence of elastic shear stiffness in the membrane shell is important for the prevention of flutter.

The method of analysis includes consideration of differential stiffness due to pre-tension and of elastic stiffness. Static pressure distribution and aerodynamic influence coefficients are computed from Newtonian impact theory.

INTRODUCTION

Large, lightly loaded atmospheric decelerators for entry from space into planetary atmospheres offer potential advantages in reduced heating rates, lower temperatures, and reduction of the decelerator weight fraction. The tension shell of flared conical shape, references 1 and 2, is a lightly loaded decelerator concept that achieves low structural weight by avoiding compressive stresses in the surface of the decelerator. Compressive loads are carried by a relatively stiff ring at the base of the shell, figure 1.

The tension shell concept is readily adapted to a deployable configuration in which the stowed volume of the decelerator is very much less than the deployed volume. In the deployable version the shell is a compliant fabric and the aft compression ring is a pressurized, filament-wound toroid illustrated in figure 1. A theoretical and experimental investigation of the deployment characteristics of flexible tension cones with

pressurized rings is reported in reference 3.

The deployable tension shell can either be attached directly to the payload or towed by a cable. Unpublished wind tunnel experiments in the Langley 6' x 9' tunnel have revealed the presence of flutter for the towed tension shell in both the rigid and the flexible versions. A theoretical investigation of the flutter of towed rigid decelerators is reported in reference 4, where it is shown that flutter can be avoided by proper placement of the center of gravity relative to the center of pressure.

The main purpose of the investigation reported here was to examine the influence of shell flexibility on flutter in the towed configuration. A secondary purpose was to develop a method of analysis that could be used for the flutter analysis of any axisymmetric decelerator system, towed or untowed, employing tensioned membranes.

SYMBOLS

Unmodified symbols:

(A^2)	parameter characterizing shape of shell
a	direction cosine
B	damping matrix
b	damping parameter
E	elastic modulus
F	component of force
G	shear modulus
K	stiffness matrix, spring constant
k	reduced frequency $(\omega R/V)$
ℓ	length
ℓ_c	length of cable

M	mass matrix
m	mass density (lb/in^2)
N	component of membrane force (lb/in)
n	number of circumferential waves
P	load
p	d/dt , pressure
q_c	force of constraint
R	base radius, also coefficient matrix for equations of constraint
r	radius from axis of symmetry
s	distance along meridian
t	shell thickness
u	component of displacement
u_s	displacement component parallel to meridian
u_φ	displacement component parallel to polar circle
V	free stream velocity
V_e	elastic strain energy
V_s	potential energy due to static preload
w	displacement component normal to surface
X	impedance matrix
y	generalized displacement
β	angle between meridian and plane normal to the axis of symmetry
Δ	difference operator

ε strain

θ rotation

ν Poisson's ratio

ρ density of atmosphere

σ stress

φ azimuth angle

ω frequency, radians/sec

Subscripts:

a index referring to position along meridian midway between mass stations

d dependent displacement component

i independent displacement component

m index referring to position along meridian at a mass station

n indicates number of circumferential waves

s in direction of meridian

w in direction of normal to surface

φ in direction of polar circle

1 indicates Fourier coefficient for $n = 1$

DESCRIPTION OF THE PROBLEM

The results of the flutter analysis of towed rigid decelerators reported in reference 4 were presented in terms of general parameters that could be applied to any decelerator configuration. The introduction of structural flexibility into the analysis makes a high degree of generality impossible because the number of

parameters required to characterize a flexible shell is large. The investigation was, accordingly, directed to the analysis of a specific configuration, shown in figure 1, that will be wind-tunnel tested.

The shroud of the model shown in figure 1 consists of Dacron structural fibers oriented along meridians and imbedded in an air-tight polyurethane sheet. The total cross-sectional area of meridional fibers is constant along the meridian. Membrane shear stiffness is provided, in an alternate design, by the addition of light weight Dacron cloth with fibers oriented 45° to the meridians.

If folding mechanics and static strength were the only considerations in the structural design of the shroud, the design with meridional fibers only would be preferable to shroud designs with fibers in two or three directions. The design with meridional fibers only provides maximum compliance in folding, and exhibits minimum structural weight. The only reason for considering designs with other fiber orientations is that flutter might thereby be suppressed.

The pressure sphere and the solenoid valve shown in figure 1 are required for inflation of the aft toroidal ring. These items of equipment were considered to be rigidly attached to the nose piece in the analysis. The aft toroidal ring was also considered to be rigid, in comparison with the cable and the flexible shroud.

Analysis of the model in figure 1 as a rigid decelerator on a flexible cable, using the method of reference 4, shows that the configuration is free from flutter for any length of cable in a Newtonian flow. Thus the presence of flutter in Newtonian flow, if detected in the present analysis, can be directly attributed to the effects of flexibility in the decelerator itself.

It is important that the same aerodynamic theory be used to calculate the static pressure distribution and the aerodynamic influence coefficients for perturbation motions. The reason is that the static pressure distribution determines the stiffening effects of pre-tension, and an inconsistency would result in the dynamic analysis if static loads and dynamic influence coefficients were computed from different theories. The static pressure distribution also determines, and must be consistent with, the shape of the shroud.

Newtonian impact theory has been used in the analysis,

primarily because its basic simplicity ensures the consistent treatment of static and dynamic pressure distributions. This may be regarded as a serious defect in the analysis because it is known that Newtonian impact theory does not accurately predict the pressure distribution on tension shell shapes, at least up to Mach 7, reference 5 . There is also evidence, reference 6, that the presence of the cable significantly alters the pressure distribution over the surface of the decelerator. The investigation and use of more advanced aerodynamic theories is a logical extension of the present study.

The problem solved in the present study was the flutter of the model shown in figure 1 for oscillations in a plane while connected to a massive body by a flexible cable. The length of the cable and the shear stiffness of the shroud were varied during the analysis. The method of analysis is described below.

METHOD OF ANALYSIS

The method of analysis was tailored to an available digital computer program, SADSAM IV, developed by the MacNeal-Schwendler Corporation. A brief account of the operating features of the program is important for an understanding of the approach taken.

SADSAM IV is a program of modest capacity (50 independent degrees of freedom) for the solution of structural dynamic problems (eigenvalue extraction, transient analysis and frequency response analysis) by the lumped element approach. A significant feature of the program is the employment of equations of constraint between dependent and independent displacement components. The general matrix equation solved by the program can be written as follows:

$$\begin{bmatrix} X_{ii} & X_{id} & -R_i^T \\ X_{di} & X_{dd} & -R_d^T \\ R_i & R_d & 0 \end{bmatrix} \begin{Bmatrix} u_i \\ u_d \\ q_c \end{Bmatrix} = \begin{Bmatrix} P_i \\ P_d \\ 0 \end{Bmatrix} \qquad (1)$$

where

u_i are independent components of displacement

u_d are dependent components of displacement

q_c are forces of constraint

The impedance matrix X_{ii} consists of mass, damping and stiffness components

$$X_{ii} = M_{ii}p^2 + B_{ii}p + K_{ii}, \qquad (2)$$

and similarly for X_{id}, X_{di}, and X_{dd}. The elements of matrices R_i and R_d are the coefficients of the equations of constraint.

The stiffness matrix K_{ii} is assembled (in part) from the properties of simple springs connected between pairs of displacement components. In addition the user can specify matrix elements to be inserted directly into K_{ii}, a feature that is used for the generation of aerodynamic force coefficients and other unconservative effects. B_{ii} and M_{ii} are assembled in similar fashion.

The coefficients of the equations of constraint, R_i and R_d in equation (1), are specified by the user to express rigid body properties of the elements of the structure and to express coordinate transformations. They may also be used, as in the present example, to express strains and rotations in terms of displacements.

The decelerator system that was analyzed consists of four parts as shown in figure 2. A single connection, representing lateral translation, is shown between the cable and the nose piece. The membrane shell has three connections, representing three orthogonal components of translation, to the nose piece and to the aft ring. Lumped element models were derived for each of the four parts and interconnected to form the complete system.

The lumped element model for the cable is very simple and therefore serves as a good introduction to the modeling technique. The model is developed in figure 3 where it is seen that the effect of tensile preload on lateral displacement of a cable element may be represented by a simple spring restraining relative lateral translation between the ends of the element. The complete model is obtained by interconnecting the springs and lumped masses for several elements.

In order to discuss the representation of the membrane shell it is first necessary to introduce the coordinate geometry and the degrees of freedom used in the analysis. Figure 4 shows the components of displacement and rotation defined at a point on the surface of the shell. The components of displacement can be expanded in terms of Fourier coefficients with respect to the azimuth coordinate, φ ,

$$\left.\begin{aligned} u_s &= u_{s_o} + \sum_{n=1}^{\infty} u_{s_n} \cdot \cos n\varphi + \sum_{n=1}^{\infty} \bar{u}_{s_n} \cdot \sin n\varphi \\ u_\varphi &= \bar{u}_{\varphi_o} + \sum_{n=1}^{\infty} u_{\varphi_n} \cdot \sin n\varphi + \sum_{n=1}^{\infty} \bar{u}_{\varphi_n} \cdot \cos n\varphi \\ w &= w_o + \sum_{n=1}^{\infty} w_n \cdot \cos n\varphi + \sum_{n=1}^{\infty} \bar{w}_n \cdot \sin n\varphi \end{aligned}\right\} \quad (3)$$

For any linear, homogeneous problem the motions corresponding to different values of n are uncoupled. Furthermore the motions corresponding to barred and unbarred Fourier coefficients are uncoupled. In the present problem we are concerned with the lateral motions of the shell as a whole which are represented by the terms corresponding to $n = 1$. Thus we specialize to the case

$$\left.\begin{aligned} u_s &= u_{s_1} \cdot \cos\varphi \\ u_\varphi &= u_{\varphi_1} \cdot \sin\varphi \\ w &= w_1 \cdot \cos\varphi \end{aligned}\right\} \quad (4)$$

The choice of unbarred coefficients indicates that $\varphi = 0$ is selected as a plane of symmetry. Every other response quantity of interest, such as an applied force or a strain, can be similarly represented as a sine or cosine function of φ, the choice being dictated by consideration of symmetry.

In the analysis the Fourier coefficients, u_{s_1}, u_{φ_1} and w_1 were selected as independent degrees of freedom. The generalized perturbation aerodynamic forces acting on them are derived in Appendix A from Newtonian impact theory. The results are expressed below as the components of generalized force acting on a strip of slant length, Δs.

$$\Delta F_{s_1} = -\pi\rho V^2 \cdot \cos^2\beta \left(\frac{\partial w_1}{\partial s} + u_{s_1} \cdot \frac{\partial \beta}{\partial s} \right) r\Delta s \tag{5}$$

$$\Delta F_{\varphi_1} = -\pi\rho V^2 \cdot \cos^2\beta \left(-w_1 + u_{\varphi_1} \cdot \sin\beta \right) \Delta s \tag{6}$$

$$\Delta F_{w_1} = -\pi\rho V^2 \left\{ \sin 2\beta \left(\frac{\partial w_1}{\partial s} + u_{s_1} \cdot \frac{\partial \beta}{\partial s} \right) + \frac{2\dot{w}_1}{V} \cdot \cos\beta - \left(\epsilon_{s_1} + \epsilon_{\varphi_1} \right) \cdot \cos^2\beta \right\} r\Delta s \tag{7}$$

The term in equation (7) proportional to the sum of membrane strains $\left(\epsilon_{s_1} + \epsilon_{\varphi_1} \right)$ represents the change in aerodynamic force due to the increase in area of a surface element. The term was not actually included in the calculation. The term proportional to $\dot{w}_1$ in equation (7) is represented by a viscous damper in the computer program. The other aerodynamic terms are incorporated in the computer solution by means of the direct input feature for matrix K_{ii} mentioned earlier.

Lumped springs and masses to represent the structural properties of the shell were derived by an energy method. The potential energy of the structure consists of a part due to elastic strain and a part due to static preload. The latter part results in a "differential stiffness" matrix similar to that for a beam-column or a rotating propeller blade. Expressions for the elastic strain energy, the potential energy due to static preload, and the kinetic

energy are derived in Appendix B. The results are expressed below for a strip of slant length Δs in terms of strains and rotations.

Elastic Strain Energy

$$\Delta V_e = \frac{\pi t r \Delta s}{2}\left[E_{ss}\left(\epsilon_{s_1} + \nu\sqrt{\frac{E_{\varphi\varphi}}{E_{ss}}}\cdot\epsilon_{\varphi_1}\right)^2 + \left(1-\nu^2\right)E_{\varphi\varphi}\epsilon^2_{\varphi_1} + G\epsilon^2_{s\varphi_1}\right] \tag{8}$$

Potential Energy due to Static Preload

$$\Delta V_s = \frac{\pi r \Delta s}{2}\left\{ N_\varphi\left[\theta^2_{s_1} + \frac{1}{r^2}\left(u_{s_1} + u_{\varphi_1}\cdot\cos\beta\right)^2\right] + N_s\left[\theta^2_{\varphi_1} + \left(\frac{\partial u_{\varphi_1}}{\partial s}\right)^2\right]\right\} \tag{9}$$

Kinetic Energy

$$\Delta T = \frac{\pi m r \Delta s}{2}\left[\dot{u}^2_{s_1} + \dot{u}^2_{\varphi_1} + \dot{w}^2_1\right] \tag{10}$$

Two simplifying assumptions were used in the calculations, namely that $E_{\varphi\varphi}$ and N_φ were zero. These assumptions are justified if the shell contains very little fiber to carry circumferential load.

The strains and rotations appearing in the above equations are related to displacements by the following formulas

$$\epsilon_{s_1} = \frac{\partial u_{s_1}}{\partial s} - w_1\cdot\frac{\partial\beta}{\partial s} \tag{11}$$

$$\epsilon_{\varphi_1} = \frac{1}{r}\left(u_{\varphi_1} + u_{s_1}\cdot\cos\beta - w_1\cdot\sin\beta\right) \tag{12}$$

$$\epsilon_{s\varphi_1} = r\cdot\frac{\partial}{\partial s}\left(\frac{u_{\varphi_1}}{r}\right) - \frac{u_{s_1}}{r} \tag{13}$$

$$\theta_{s_1} = \frac{1}{r}\left[- w_1 + u_{\varphi_1} \cdot \sin\beta \right] \tag{14}$$

$$\theta_{\varphi_1} = - \frac{\partial w_1}{\partial s} - u_{s_1} \cdot \frac{\partial \beta}{\partial s} \tag{15}$$

It will be noted that the strain and potential energy formulas are expressed in the form

$$\Delta V = \frac{1}{2} \cdot \sum_i \cdot K_i \left(y_i \right)^2 \tag{16}$$

where y_i is a generalized displacement quantity related to the actual components of displacement by a linear operator. Hence K_i represents a spring restraining y_i and it is represented as such in the computer program. The relationship between each y_i and the components of displacement is regarded as an equation of constraint. Differential operators occuring in the equations of constraint are replaced by finite difference operators. For example, in the term proportional to $\theta^2_{\varphi_1}$ in equation (9),

$$y_i = - \theta_{\varphi_i} = \frac{\partial w_1}{\partial s} + u_{s_1} \cdot \frac{\partial \beta}{\partial s} = \frac{1}{\Delta s}\left(w_{m+1} - w_m \right) + \frac{1}{2} \cdot \frac{\partial \beta}{\partial s}\left(u_{s_{m+1}} + u_{s_m} \right) \tag{17}$$

where the indices m and m+1 refer to adjacent stations along the meridian of the shell.

The module that represents the mechanical properties of a section of shell consists of the springs, K_i, the equations of constraint and the mass coefficients indicated by equation (10). A diagram representing the module is shown in figure 5. Formulas for the values of the elements in the module are contained in Appendix C.

It will be noted in figure 5 that some springs are connected

at stations (K_2 , K_4 , and K_5) and some springs are connected between stations (K_1 , K_3 , K_6 , and K_7). A spring connected between stations contains a derivative with respect to distance along the meridian in its equation of constraint, while a spring connected at a station does not. In the calculation all of the springs located at stations were null due to the assumption that $E_{\varphi\varphi}$ and N_φ are zero.

The complete lumped element model for the membrane shell is formed by joining the modules for individual sections together and specifying the aerodynamic force coefficients. The models to represent the nose piece and the rigid aft ring consist of lumped masses and the equations of constraint required to form the relationships between their motions and the components of displacement at the connection points with the other parts of the system. The nose piece also includes a spring to represent the effect of axial pre-tension between the cable attachment point and the point of connection to the membrane shell.

A diagram showing the detailed model for the complete system is shown in figure 6. The model includes the mechanical springs and masses discussed above, viscous dampers that simulate aerodynamic damping, and the direct input aerodynamic stiffness terms.

Once the model has been completed and its properties coded into the computer program, the eigenvalues and eigenvectors that describe the aerodynamically damped modes of the system are computed by a subroutine.

RESULTS OF NUMERICAL CALCULATION

The method described above was applied to the flexible tension shell decelerator shown in figure 1. The model used for the numerical calculations included eight cable segments and eight membrane shell segments (see fig. 6). Since the shell is flexible, the exact equilibrium shape of the shroud depends on the static aerodynamic pressure distribution. Shell shapes for Newtonian flow with zero stress in the circumferential direction are defined in reference 2, in terms of a parameter (A^2) that depends on the ratio of shell height to base radius. For the present example a value $A^2 = 1.4$, was selected. The meridional force coefficient is given by

$$N_s = \frac{\rho V^2 R^2}{2(A^2)r} \tag{18}$$

where R is the base radius. N_φ is zero.

In order to permit scaling of the results to other shells, the parameters describing the decelerator are expressed in dimensionless form. The values of pertinent parameters used in the analysis are listed in Table I.

The aerodynamic mass parameter determines the magnitude of the aerodynamic damping. It probably has a negligible effect on flutter criteria. The value shown in Table I is representative of operation of the model in a wind tunnel at Mach 4 and 2000 psf dynamic pressure.

The meridional strain parameter determines the relative magnitude of elastic stiffness compared to the stiffening effects of perturbation aerodynamic forces and static preload. The value selected is representative of the fiber used in the shroud of the model.

Two values of the ratio of the shear modulus to the meridional elastic modulus were investigated. The value $G/E_{ss} = 0$ corresponds to a shroud in which meridional fibers are held in place by a complaint matrix. The value $G/E_{ss} = 0.1$ corresponds to a shroud with some helically wound fibers as well as meridional fibers.

The length of the cable was varied parametrically since it was known from previous work on the flutter of rigid decelerators, reference 5, that cable length is an important parameter for flutter.

The results of the analysis are the frequency and damping of the aerodynamically damped vibration modes and the corresponding mode shapes. Damping and frequency are expressed as the real and imaginary parts of the eigenvalue

$$\lambda = \alpha + i\omega = \frac{V}{R}(b + ik) \qquad (19)$$

The dimensionless parameter $k = \frac{\omega R}{V}$ is the conventional reduced frequency, or Strouhal number, used to express the results of flutter analysis.

The damping and frequency obtained for the four lowest modes

of the decelerator are presented as root locus plots in figures 7a and 7b. The varied parameter is the ratio of cable length to decelerator base radius. The model with shear stiffness is seen to be stable in all modes for all cable lengths, while the model without shear stiffness becomes slightly unstable in its second mode for a small range of cable lengths, $9.5 < \ell_c/_R < 12$. The flutter is associated with the coalescence of the frequencies of the second and third modes.

A tendency for the root of a mode to track the root of the next lower mode at a larger cable length is evident in figure 7. The tendency occurs because the impedances that two cables present to the decelerator at a given frequency are the same if the number of half-wavelengths along the cables differ by an integer, (see reference 5).

Mode shapes are plotted in figures 8 to 11 for the first four modes with $\ell_c/R = 6$. The first four modes are primarily combinations of the following deformations

- rigid translation of the decelerator
- rigid rotation of the decelerator
- shearing distortion of the shroud near the nose piece
- cable whipping with 1/2 to 3/4 wavelength.

Shearing distortion of the shroud is quite prominent in the second mode of the decelerator without elastic shear stiffness, and in the third mode of the decelerator with elastic shear stiffness.

The second mode of the decelerator without elastic shear stiffness is plotted in figure 12, for a cable length in the flutter region. The only prominent difference from the stable condition ($\ell_c/R = 6$) is that rigid pitching of the decelerator is absent.

The mode shape for the sixth mode of the decelerator without elastic shear stiffness is shown in figure 13. Normal displacements (w) in the plane $\varphi = 0$, as well as tangential displacements (u_φ) for $\varphi = \pi/2$, are plotted. This mode, which was relatively heavily damped, is the lowest that includes large rotation of the aft ring relative to the shroud. The addition of

elastic shear stiffness had very little effect on the frequency or damping.

CONCLUDING DISCUSSION

The analysis described above shows that the effects of flexibility can produce flutter in a towed decelerator that would be stable if it were rigid. The type of flutter that was detected is characterized by the coalescence of the frequencies of a pair of modes, and by the presence of shearing distortion in the shell. The flutter was eliminated by the addition of elastic shearing stiffness to the shell.

One of the reasons that shear flexibility is significant for the model studied is that the radius of the shell at the attachment to the nose piece is small. The mode shapes (figures 8 to 12) show that all of the shear deformation occurs within a short distance of the nose piece. The effect of shear flexibility can, therefore, be reduced by increasing the size of the nose piece.

It is unlikely that the quantitative results of the analysis will be supported by wind tunnel tests due to the use of Newtonian flow theory in the analysis. Further analytical effort on the problem should include a consideration of more advanced aerodynamic theories.

The method of analysis developed during the investigation is applicable to the aeroelastic analysis of any axisymmetric decelerator system, towed or untowed, employing tensioned membranes. It can, for example, be used to study the panel flutter of an untowed tension shell used as a reentry decelerator. The application of Newtonian impact theory is a less serious assumption for this example due to the high Mach number at peak deceleration and the absence of flow disturbances produced by a tow cable.

Astro Research Corporation
Santa Barbara, California, October 18, 1966.

APPENDIX A.

AERODYNAMIC FORCE COEFFICIENTS

The aerodynamic pressure acts normal to a solid surface in Newtonian flow and its magnitude is given by

$$p = \rho V_p^2 \qquad A(1)$$

where ρ is the density and V_p is the component of flow normal to the surface in the free stream.

Consider an element of a surface of revolution shown in Figure 4. The velocity normal to the surface is, considering terms to first order in the motions

$$V_p = V \cdot \cos\left(\beta - \theta_\varphi\right) - \dot{w} \qquad A(2)$$

(See list of symbols for definitions.)

Substitute Equation A(2) into Equation A(1) and expand

$$p = \rho\left[V^2 \cdot \cos^2\left(\beta - \theta_\varphi\right) - 2V\dot{w} \cdot \cos\left(\beta - \theta_\varphi\right) + \dot{w}^2\right] \qquad A(3)$$

Now, considering $\theta_\varphi << \beta$

$$\cos\left(\beta - \theta_\varphi\right) = \cos\beta + \theta_\varphi \cdot \sin\beta \qquad A(4)$$

$$\cos^2\left(\beta - \theta_\varphi\right) = \cos^2\beta + \theta_\varphi \cdot \sin 2\beta \qquad A(5)$$

correct to first order in θ_φ. Substitute into Equation A(3) and keep terms to first order in θ_φ and $\dot{w}$.

$$p = \rho \left\{ V^2 \cdot \cos^2\beta + V^2 \cdot \sin(2\beta) \cdot \theta_\varphi - 2V\dot{w} \cdot \cos\beta \right\} \qquad A(6)$$

The direction cosines of the normal to the deflected surface in the u_s , u_φ and w directions are, to first order in the motions,

$$\left.\begin{aligned} a_s &= \theta_\varphi \\ a_\varphi &= -\theta_s \\ a_w &= 1 \end{aligned}\right\} \qquad A(7)$$

The components of pressure in the u_s , u_φ and w directions are, to first order in the motions

$$p_s = a_s p = + \rho V^2 \cdot \cos^2\beta \cdot \theta_\varphi \qquad A(8)$$

$$p_\varphi = a_\varphi p = - \rho V^2 \cdot \cos^2\beta \cdot \theta_s \qquad A(9)$$

$$p_w = a_w p = \rho \left\{ V^2 \cdot \cos^2\beta + V^2 \cdot \sin 2\beta \cdot \theta_\varphi - 2V\dot{w} \cdot \cos\beta \right\} \qquad A(10)$$

The element of area on which the pressure acts is

$$dA = \left(1 + \epsilon_s\right) \cdot \left(1 + \epsilon_\varphi\right) r d\varphi ds \qquad A(11)$$

The strains ϵ_s and ϵ_φ are included to account for an increase in area due to stretching.

The rotations θ_s and θ_φ are related to displacements as follows

$$\theta_s = \frac{1}{r}\cdot\frac{\partial w}{\partial \varphi} + \frac{u_\varphi}{r}\cdot\sin\beta \qquad A(12)$$

$$\theta_\varphi = -\frac{\partial w}{\partial s} - u_s\cdot\frac{\partial \beta}{\partial s} \qquad A(13)$$

so that Equations A(8), and A(9) become

$$p_s = -\rho V^2\cdot\cos^2\beta\left[\frac{\partial w}{\partial s} + u_s\cdot\frac{\partial \beta}{\partial s}\right] \qquad A(14)$$

and

$$p_\varphi = -\rho V^2\cdot\cos^2\beta\left[\frac{1}{r}\cdot\frac{\partial w}{\partial \varphi} + \frac{u_\varphi}{r}\cdot\sin\beta\right] \qquad A(15)$$

The displacements are assumed to depend on the azimuth angle φ in the following manner (see eqn. 4 of text).

$$u_s = u_{s_1}\cdot\cos\varphi \qquad A(16)$$

$$u_\varphi = u_{\varphi_1}\cdot\sin\varphi \qquad A(17)$$

$$w = w_1\cdot\cos\varphi \qquad A(18)$$

Regarding u_{s_1}, u_{φ_1}, and w_1, as generalized coordinates, the corresponding generalized forces are

$$F_{s_1} = \int_A \cos\varphi\cdot p_s\, dA \qquad A(19)$$

$$F_{\varphi_1} = \int_A \sin\varphi \cdot p_\varphi dA \qquad A(20)$$

$$F_{w_1} = \int_A \cos\varphi \cdot p_w dA \qquad A(21)$$

The calculation of aerodynamic coefficients is completed by substituting previously derived expressions for the components of pressure and for dA into these equations and integrating over the surface of a strip of slant length Δs. In the calculation only the terms of first order in the motions are retained. As a result the strains, ϵ_s and ϵ_φ, are retained only in Equation A(21).

The results of the calculation are

$$\Delta F_{s_1} = -\pi\rho V^2 \cdot \cos^2\beta \left(\frac{\partial w_1}{\partial s} + u_{s_1} \cdot \frac{\partial \beta}{\partial s} \right) r\Delta s \qquad A(22)$$

$$\Delta F_{\varphi_1} = -\pi\rho V^2 \cdot \cos^2\beta \left(-w_1 + u_{\varphi_1} \cdot \sin\beta \right) \Delta s \qquad A(23)$$

$$\Delta F_{w_1} = -\pi\rho V^2 \left\{ \sin 2\beta \left(\frac{\partial w_1}{\partial s} + u_{s_1} \cdot \frac{\partial \beta}{\partial s} \right) + \frac{2\dot{w}_1}{V} \cdot \cos\beta - \left(\epsilon_{s_1} + \epsilon_{\varphi_1} \right) \cos^2\beta \right\} r\Delta s \qquad A(24)$$

APPENDIX B.

ENERGY EXPRESSIONS

Elastic Strain Energy of an Orthotropic Membrane of Revolution

The components of membrane strain in the coordinate system depicted in Figure 4 are

$$\epsilon_s = \frac{\partial u_s}{\partial s} - w \cdot \frac{\partial \beta}{\partial s} \qquad B(1)$$

$$\epsilon_\varphi = \frac{1}{r} \cdot \frac{\partial u_\varphi}{\partial \varphi} + \frac{u_s \cdot \cos\beta - w \cdot \sin\beta}{r} \qquad B(2)$$

$$\epsilon_{s\varphi} = r \cdot \frac{\partial}{\partial s}\left(\frac{u_\varphi}{r}\right) + \frac{1}{r} \cdot \frac{\partial u_s}{\partial \varphi} \qquad B(3)$$

The stress-strain relationships for an orthotropic membrane are

$$\begin{Bmatrix} \sigma_s \\ \sigma_\varphi \\ \sigma_{s\varphi} \end{Bmatrix} = \left[\begin{array}{cc|c} E_{ss} & E_{s\varphi} & 0 \\ E_{s\varphi} & E_{\varphi\varphi} & 0 \\ \hline 0 & 0 & G \end{array}\right] \begin{Bmatrix} \epsilon_s \\ \epsilon_\varphi \\ \epsilon_{s\varphi} \end{Bmatrix} \qquad B(4)$$

Alternatively we may replace $E_{s\varphi}$ by $\sqrt{E_{ss}\, E_{\varphi\varphi}} \cdot \nu$ where ν is an effective Poisson's ratio. The strain energy per unit area is

$$\delta V_e = \frac{1}{2}\left[\sigma_s \epsilon_s + \sigma_\varphi \epsilon_\varphi + \sigma_{s\varphi} \epsilon_{s\varphi}\right] t \cdot r\, d\varphi\, ds \qquad B(5)$$

where t is the thickness of the membrane.

Substituting from Equation B(4) into Equation B(5)

$$\delta V_e = \frac{1}{2}\left[E_{ss}\cdot\epsilon_s^2 + 2E_{s\varphi}\epsilon_s\epsilon_\varphi + E_{\varphi\varphi}\epsilon_\varphi^2 + G\epsilon_{s\varphi}^2\right]trd\varphi ds \qquad B(6)$$

Express the strains in terms of sine and cosine components for a plane of symmetry at $\varphi = 0$

$$\epsilon_s = \epsilon_{s_1}\cdot\cos\varphi \qquad B(7)$$

$$\epsilon_\varphi = \epsilon_{\varphi_1}\cdot\cos\varphi \qquad B(8)$$

$$\epsilon_{s\varphi} = \epsilon_{s\varphi_1}\cdot\sin\varphi \qquad B(9)$$

Then, substituting these relationships into the definition of strain, Equations B(1), B(2), and B(3),

$$\epsilon_{s_1} = \frac{\partial u_{s_1}}{\partial s} - w_1\cdot\frac{\partial\beta}{\partial s} \qquad B(10)$$

$$\epsilon_{\varphi_1} = \frac{1}{r}\cdot u_{\varphi_1} + \frac{u_{s_1}\cdot\cos\beta - w_1\cdot\sin\beta}{r} \qquad B(11)$$

$$\epsilon_{s\varphi_1} = r\cdot\frac{\partial}{\partial s}\left(\frac{u_{\varphi_1}}{r}\right) - \frac{u_{s_1}}{r} \qquad B(12)$$

The strain energy of a strip of slant length Δs is obtained

by substituting Equations B(7), B(8), and B(9) into Equation B(6) and integrating with respect to φ . The result is

$$\Delta V_e = \frac{\pi tr\Delta s}{2}\left[E_{ss}\epsilon^2_{s_1} + 2E_{s\varphi}\epsilon_{s_1}\epsilon_{\varphi_1} + E_{\varphi\varphi}\epsilon^2_{\varphi_1} + G\epsilon^2_{s\varphi_1}\right] \qquad B(13)$$

It is convenient to express ΔV_e as a sum of squares. Using $E_{s\varphi} = \nu\sqrt{E_{ss}E_{\varphi\varphi}}$, the result is

$$\Delta V_e = \frac{\pi tr\Delta s}{2}\left[E_{ss}\left(\epsilon_{s_1} + \nu\sqrt{\frac{E_{\varphi\varphi}}{E_{ss}}}\cdot\epsilon_{\varphi_1}\right)^2 + (1-\nu^2)E_{\varphi\varphi}\epsilon^2_{\varphi_1} + G\epsilon^2_{s\varphi_1}\right] \qquad B(14)$$

Potential Energy of a Membrane of Revolution Due to Static Preload

Consider a small element of a membrane, shown below, in static equilibrium under tensions N_s and N_φ .

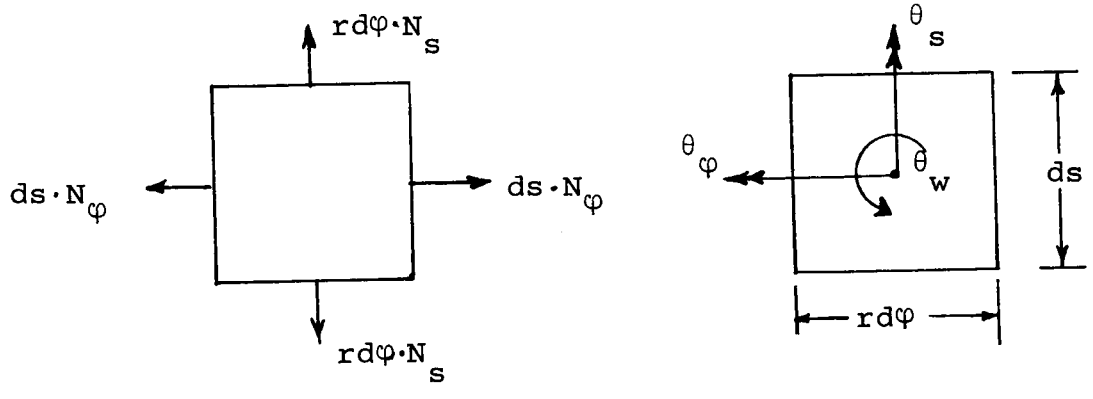

In order to calculate the work done by preload, consider a virtual motion in which the preload forces N_s and N_φ remain attached to the element, move with it, and remain fixed in magnitude and direction, when the element is moved or distorted. The forces will, consequently, remain in equilibrium with the applied external loads. It is necessary to consider only second order terms in computing the motions.

The basis of the calculation is as follows: If a rigid bar of length ℓ subjected to end load P is rotated thru an angle θ, the work done against the load P is

$$V_s = \ell P(1 - \cos\theta) \simeq \frac{1}{2}\cdot \ell P\theta^2 \qquad B(15)$$

V_s is the increase in potential energy of the bar. Consider next a bar that is rotated about two perpendicular axes as shown below

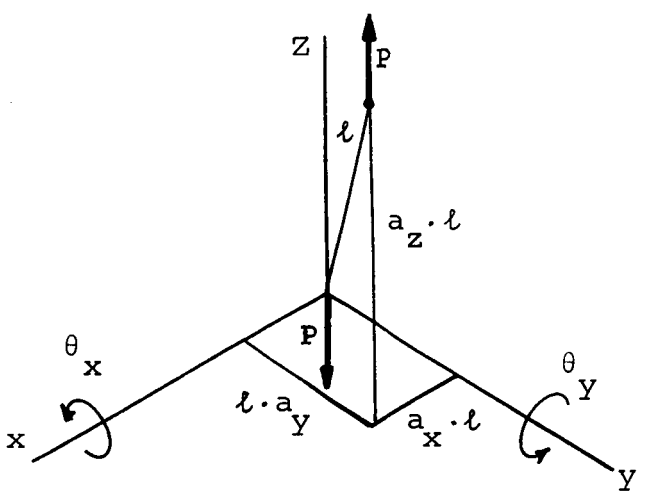

The work done against the end load P is

$$V_s = P\ell\left(1 - a_z\right) \qquad B(16)$$

where a_z is the direction cosine of the rotated bar in the z - direction. Now

$$a_x^2 + a_y^2 + a_z^2 = 1 \qquad B(17)$$

so that

$$1 - a_z = 1 - \sqrt{1 - a_x^2 - a_y^2} \qquad B(18)$$

$$\simeq \frac{1}{2}\left(a_x^2 + a_y^2\right)$$

correct to third order in a_x and a_y.

Also

$$a_x^2 = \theta_y^2 \qquad B(19)$$

$$a_y^2 = \theta_x^2 \qquad B(20)$$

correct to second order in θ_x and θ_y.

Hence

$$V_s = \frac{1}{2} \cdot P\ell \left(\theta_x^2 + \theta_y^2 \right) \qquad B(21)$$

correct to second order in θ_x and θ_y .

In order to apply the above theory to a membrane, it is convenient to regard the membrane as composed of rigid bars that are free to rotate in all directions as shown below.

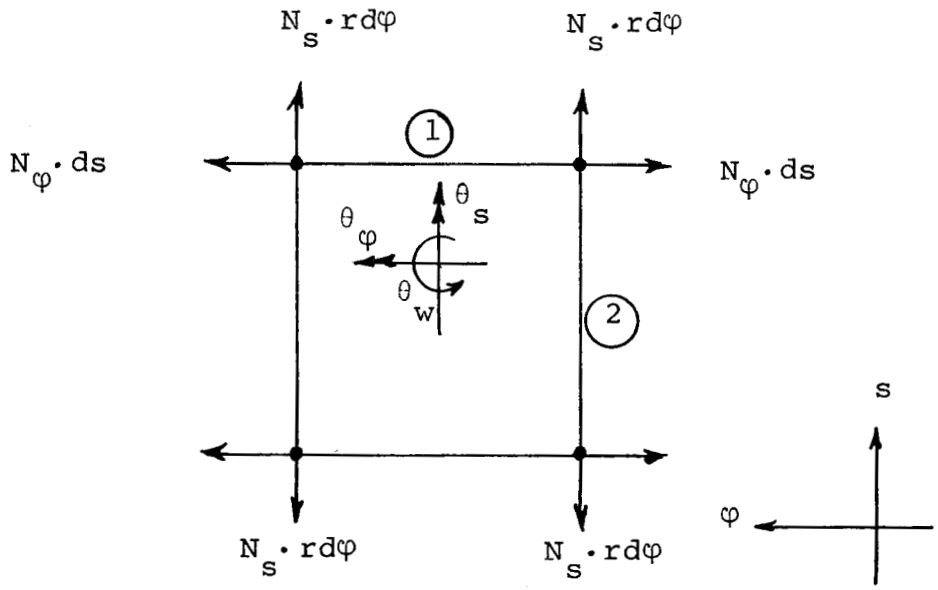

The out-of-plane rotations of bars ① and ② are θ_s and θ_φ respectively. The in-plane rotations of bars ① and ② include contributions from the shear strain as well as from the rigid body rotation θ_w as shown below.

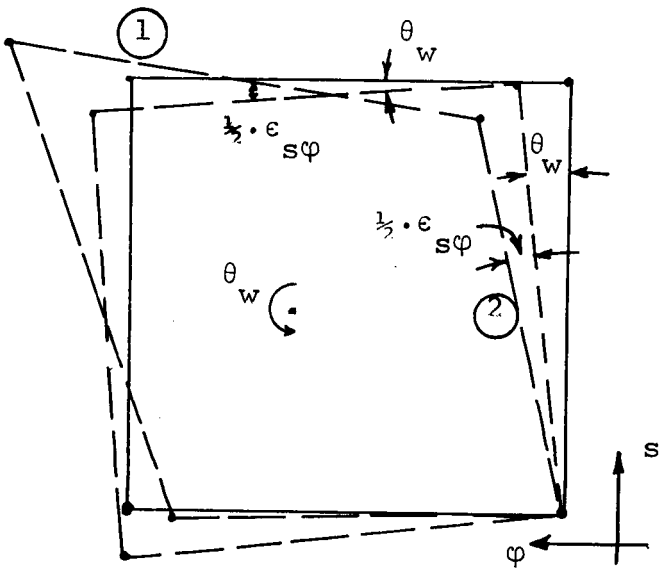

The in-plane rotations of bars ① and ② are respectively

$$\theta_{1i} = \theta_w - \frac{1}{2}\cdot\epsilon_{s\varphi} \qquad \text{B(22)}$$

$$\theta_{2i} = \theta_w + \frac{1}{2}\cdot\epsilon_{s\varphi} \qquad \text{B(23)}$$

The potential energy density per unit area is, using Equation B(21),

$$\delta V_s = \frac{1}{2}\cdot r d\varphi ds\left\{N_\varphi\left[\theta_s^2 + \left(\theta_w - \frac{1}{2}\cdot\epsilon_{s\varphi}\right)^2\right] + N_s\left[\theta_\varphi^2 + \left(\theta_w + \frac{1}{2}\cdot\epsilon_{s\varphi}\right)^2\right]\right. \qquad \text{B(24)}$$

Expressions for the rotations and shear strain in terms of displacements are presented in Reference 7. They are

$$\epsilon_{s\varphi} = r\cdot\frac{\partial}{\partial s}\left(\frac{u_\varphi}{r}\right) + \frac{1}{r}\cdot\frac{\partial u_s}{\partial \varphi} \qquad \text{B(25)}$$

$$\theta_s = \frac{1}{r}\cdot\frac{\partial w}{\partial \varphi} + \frac{u_\varphi}{r}\cdot\sin\beta \qquad \text{B(26)}$$

$$\theta_\varphi = -\frac{\partial w}{\partial s} - u_s\cdot\frac{\partial \beta}{\partial s} \qquad \text{B(27)}$$

$$\theta_w = \frac{1}{2r}\left\{\frac{\partial\left(ru_\varphi\right)}{\partial s} - \frac{\partial u_s}{\partial \varphi}\right\} \qquad \text{B(28)}$$

From these expressions, it can be shown by straightforward substitution that

$$\theta_w - \frac{1}{2}\cdot\epsilon_{s\varphi} = \frac{1}{r}\left[u_\varphi\cdot\cos\beta - \frac{\partial u_s}{\partial \varphi}\right] \qquad \text{B(29)}$$

and

$$\theta_w + \frac{1}{2}\cdot\epsilon_{s\varphi} = \frac{\partial u_\varphi}{\partial s} \qquad \text{B(30)}$$

With these expressions the potential energy density becomes

$$\delta V_s = \frac{1}{2}\cdot r\,d\varphi\,ds\left\{N_\varphi\left[\theta_s^2 + \frac{1}{r^2}\left(\frac{\partial u_s}{\partial \varphi} - u_\varphi\cos\beta\right)^2\right] + N_s\left[\theta_\varphi^2 + \left(\frac{\partial u_\varphi}{\partial s}\right)^2\right]\right\} \qquad \text{B(31)}$$

Express the rotations and displacements in terms of sine and cosine components for a plane of symmetry at $\varphi = 0$

$$\left.\begin{aligned} \theta_s &= \theta_{s_1} \cdot \sin\varphi \\ \theta_\varphi &= \theta_{\varphi_1} \cdot \cos\varphi \\ u_s &= u_{s_1} \cdot \cos\varphi \\ u_\varphi &= u_{\varphi_1} \cdot \sin\varphi \end{aligned}\right\} \qquad \text{B(32)}$$

The desired expression for potential energy of a strip of slant length Δs is obtained by substituting these expressions into Equation B(31) and integrating with respect to φ. The result is

$$\Delta V_s = \frac{\pi r \Delta s}{2}\left\{ N_\varphi\left[\theta_{s_1}^2 + \frac{1}{r^2}\left(u_{s_1} + u_{\varphi_1}\cdot\cos\beta\right)^2\right] + N_s\left[\theta_{\varphi_1}^2 + \left(\frac{\partial u_{\varphi_1}}{\partial s}\right)^2\right]\right\} \qquad \text{B(33)}$$

Kinetic Energy of a Membrane of Revolution

The kinetic energy density is

$$\delta T = \frac{1}{2}\cdot m\left(\dot{u}_s^2 + \dot{u}_\varphi^2 + \dot{w}^2\right) \qquad \text{B(34)}$$

Express u_s, u_φ, and w in terms of sine and cosine components of the azimuth angle as before. The kinetic energy of a strip of slant length Δs is

$$\Delta T = \frac{\pi}{2}\cdot mr\Delta s\left[\dot{u}_{s_1}^2 + \dot{u}_{\varphi_1}^2 + \dot{w}_1^2\right] \qquad \text{B(35)}$$

where m is the mass per unit area.

APPENDIX C.

FORMULAS FOR ELEMENTS IN THE MODULE

REPRESENTING A SECTION OF MEMBRANE SHELL

Formulas for the elements are presented with reference to Figure 5 , the diagram for the module.

Masses

$$m_1 = m_2 = m_3 = \pi m r \Delta s_m$$

Viscous Damper

$$B_1 = 2\pi\rho V \cdot \cos\beta \cdot r \Delta s_m$$

Springs

$$K_1 = \pi t r \Delta s_a E_{ss}$$

$$K_2 = \pi t r \Delta s_m \left(1 - \nu^2\right) E_{\varphi\varphi}$$

$$K_3 = \pi t r \Delta s_a G$$

$$K_4 = \pi r \Delta s_m N_\varphi$$

$$K_5 = \pi r \Delta s_m N_\varphi$$

$$K_6 = \pi r \Delta s_a N_s$$

$$K_7 = \frac{\pi r}{\Delta s_a} \cdot N_s$$

Constraint Equations

$$y_1 = \epsilon_s + \nu\sqrt{\frac{E_{\varphi\varphi}}{E_{ss}}}\cdot\epsilon_\varphi$$

$$= a_1 w_{m+1} + a_2 w_m + a_3 u_{s,m+1} + a_4 u_{sm} + a_5 u_{\varphi,m+1} + a_6 u_{\varphi,m}$$

where:

$$a_1 = a_2 = -\frac{1}{2}\left[\frac{\partial\beta}{\partial s} + \frac{\nu}{r_a}\sqrt{\frac{E_{\varphi\varphi}}{E_{ss}}}\cdot\sin\beta\right]$$

$$a_3 = \frac{1}{\Delta s_a} + \frac{\nu}{2r_a}\sqrt{\frac{E_{\varphi\varphi}}{E_{ss}}}\cdot\cos\beta$$

$$a_4 = \frac{-1}{\Delta s_a} + \frac{\nu}{2r_a}\sqrt{\frac{E_{\varphi\varphi}}{E_{ss}}}\cdot\cos\beta$$

$$a_5 = a_6 = \frac{\nu}{2r_a}\sqrt{\frac{E_{\varphi\varphi}}{E_{ss}}}$$

$$y_2 = \epsilon_\varphi = b_2 w_m + b_4 u_{s,m} + b_6 u_{\varphi,m}$$

where:

$$b_2 = \frac{-\sin\beta}{r_m}$$

$$b_4 = \frac{\cos\beta}{r_m}$$

$$b_6 = \frac{1}{r_m}$$

$$y_3 = \epsilon_{s\varphi} = c_3 u_{s,m+1} + c_4 u_{s,m} + c_5 u_{\varphi,m+1} + c_6 u_{\varphi,m}$$

where:

$$c_3 = c_4 = \frac{-1}{2r_a}$$

$$c_5 = \frac{1}{\Delta s_a} \cdot \frac{r_a}{r_{m+1}}$$

$$c_6 = \frac{-1}{\Delta s_a} \cdot \frac{r_a}{r_m}$$

$$y_4 = \theta_s = d_2 w_m + d_6 u_{\varphi,m}$$

where:

$$d_2 = \frac{-1}{r_m}$$

$$d_6 = \frac{\sin\beta}{r_m}$$

$$y_5 = \frac{1}{r}\left(u_s + u_\varphi \cdot \cos\beta\right)$$

$$= e_4 u_{s,m} + e_6 u_{\varphi,m}$$

where:

$$e_4 = \frac{1}{r_m}$$

$$e_6 = \frac{\cos\beta}{r_m}$$

$$y_6 = -\theta_\varphi = f_1 w_{m+1} + f_2 w_m + f_3 u_{s,m+1} + f_4 u_{s,m}$$

where:

$$f_1 = \frac{1}{\Delta s_a}$$

$$f_2 = \frac{-1}{\Delta s_a}$$

$$f_3 = f_4 = \frac{1}{2} \cdot \frac{\partial\beta}{\partial s}$$

Direct Input Aerodynamic Force Coefficients

The perturbation aerodynamic forces at the mth station, excluding the viscous damper term simulated by B_1 and the terms proportional to strains, are:

$$\begin{Bmatrix} \Delta F_{s,m} \\ \Delta F_{\varphi,m} \\ \Delta F_{w,m} \end{Bmatrix} = -\pi\rho V^2 r_m \Delta s_m \left[\begin{array}{c|c|c|c|c} A_{11} & 0 & 0 & A_{14} & A_{15} \\ \hline 0 & A_{22} & A_{23} & 0 & 0 \\ \hline A_{31} & 0 & 0 & A_{34} & A_{35} \end{array}\right] \left\{\begin{array}{c} u_{s,m} \\ \hline u_{\varphi,m} \\ \hline w_m \\ \hline w_{m+1} \\ \hline w_{m-1} \end{array}\right\}$$

The A's are the coefficients of a stiffness matrix $\left[K_{ij}\right]$ such that

$$\left[K_{ij}\right] = \pi\rho V^2 r_m \Delta s_m \left[A_{ij}\right]$$

where

$$A_{11} = \cos^2\beta \cdot \frac{\partial\beta}{\partial s}$$

$$A_{14} = -A_{15} = \left(\cos^2\beta\right)/2\Delta s_m$$

$$A_{22} = \left(\cos^2\beta \cdot \sin\beta\right)/r_m$$

$$A_{23} = -\left(\cos^2\beta\right)/r_m$$

$$A_{31} = \sin 2\beta \cdot \frac{\partial\beta}{\partial s}$$

$$A_{34} = -A_{35} = \left(\sin 2\beta\right)/2\Delta s_m$$

REFERENCES

1. Anderson, Roger A.: Structures Technology - 1964. Astronaut. Aeron., vol. 2, no. 12, Dec. 1964, pp. 14-20.

2. Anderson, M. S.; Robinson, J. C.; Bush, H. G.; and Fralich, R. W.: A Tension Shell Structure For Application to Entry Vehicles. NASA TN D-2675, 1965.

3. Kyser, A. C.: Deployment Mechanics for an Inflatable Tension-Shell Decelerator. NASA CR (To be assigned.)

4. MacNeal, R. H.: The Flutter of Towed Rigid Decelerators. NASA CR-766, 1967.

5. Robinson, J. C.; and Jordan, A. W.: Exploratory Experimental Aerodynamic Investigation of Tension Shell Shapes at Mach 7. NASA TN D-2994, 1965.

6. Charczenko, N.; and McShera, J. T.: Aerodynamic Characteristics of Towed Cones Used as Decelerators at Mach Numbers from 1.57 to 4.65. NASA TN D-994, 1961.

7. MacNeal, R. H.: Mechanics of a Coned Rotating Net. NASA CR-248, 1965.

TABLE I

PARAMETERS DESCRIBING DECELERATOR

Cable weight	$\frac{W_{cable}}{W_{decelerator}} = .03\left(\frac{\ell_c}{R}\right)$
Aerodynamic mass parameter	$\frac{\rho R^3}{m_{decelerator}} = .01$
Meridional strain under static load	$\epsilon_s = \frac{\sigma_s}{E_{ss}} = .01$
Ratios of elastic moduli	$E_{\varphi\varphi}/E_{ss} = 0$
	$G/E_{ss} = 0$ (Case B)
	$= 0.1$ (Case A)
Cable length	$\frac{\ell_c}{R} = 3,4,5,6,7,8,9,10,11,12$ (Values used)

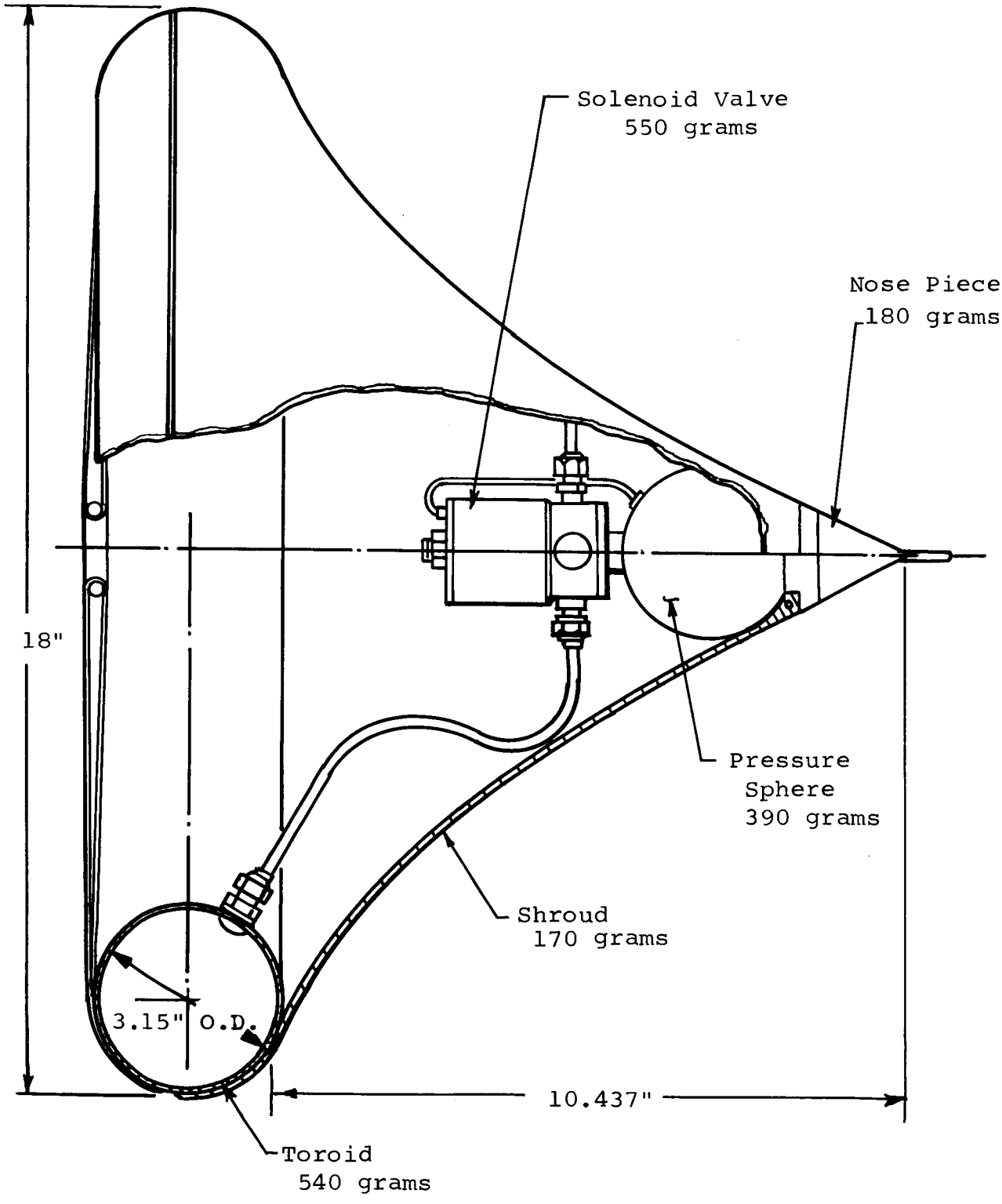

Figure 1. — Flexible Tension Shell

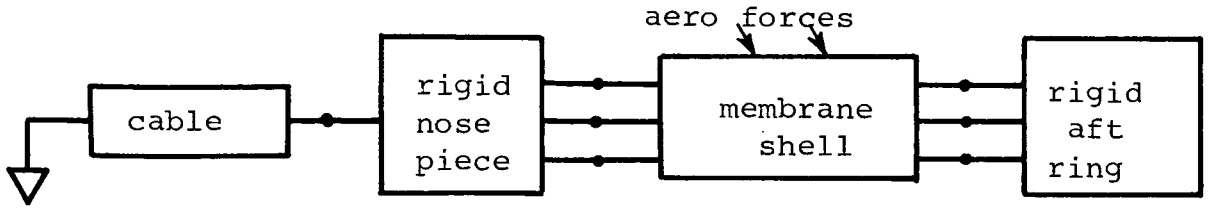

Figure 2. — Block Model of Decelerator System

Moment Equilibrium

$$F_2 = -F_1 = \frac{T}{\Delta \ell}\left(u_2 - u_1\right)$$

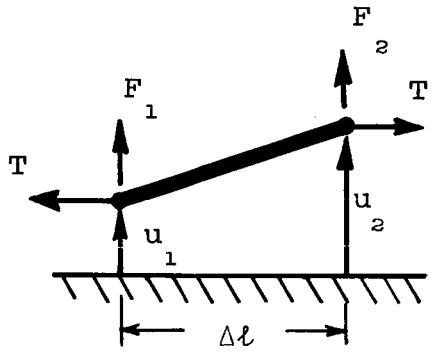

(a) Equilibrium of displaced cable element

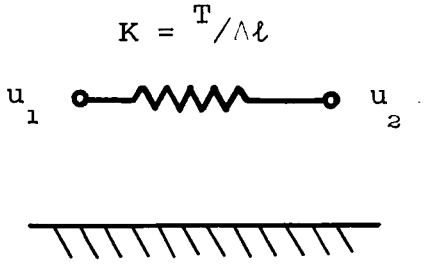

(b) Lumped spring model for cable element

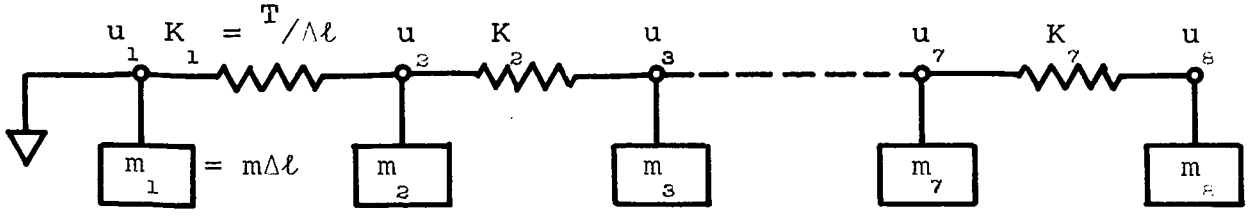

(c) Model for complete cable

Figure 3. — Development of Model for Cable

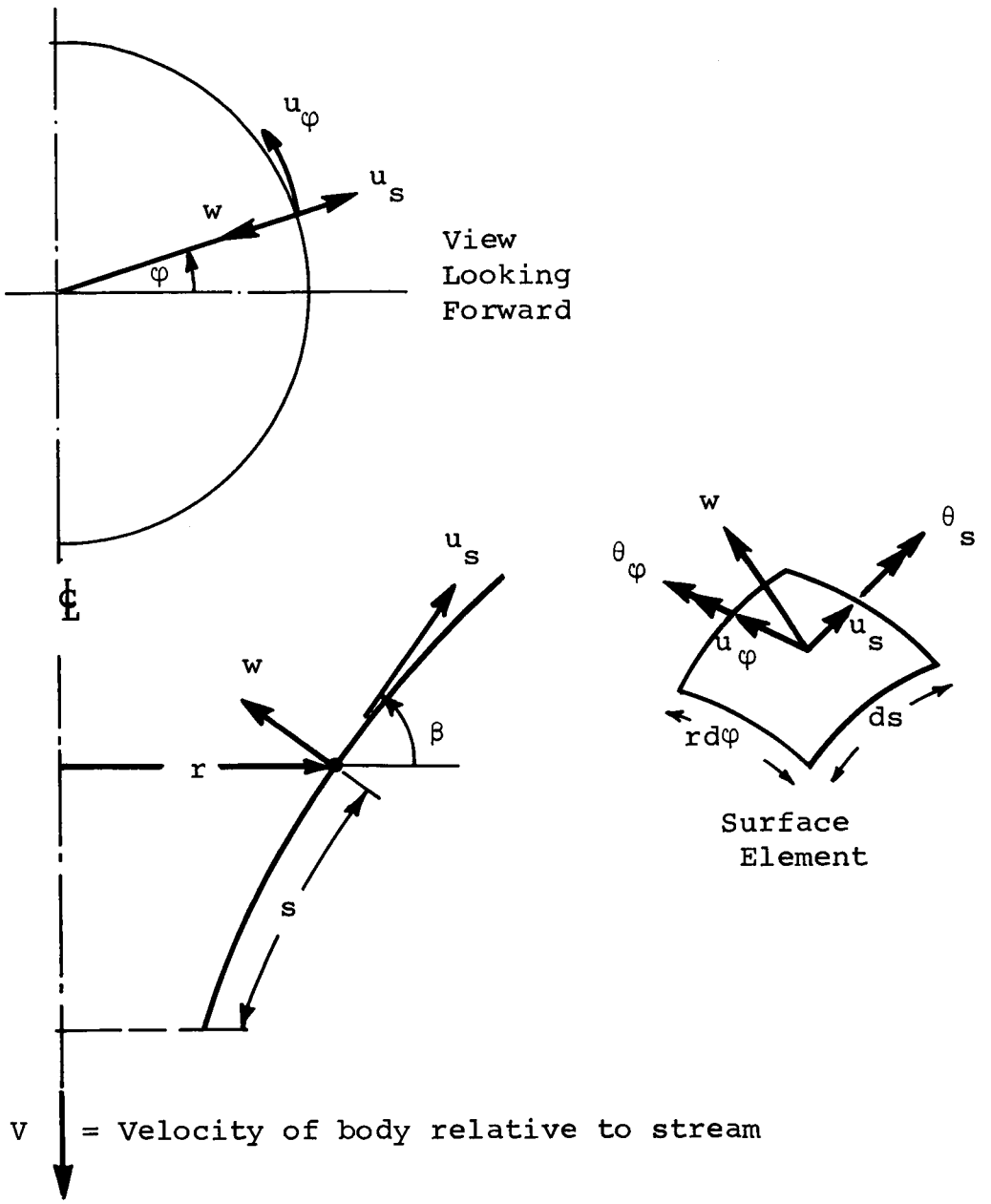

Figure 4. — Coordinate Geometry of Shell

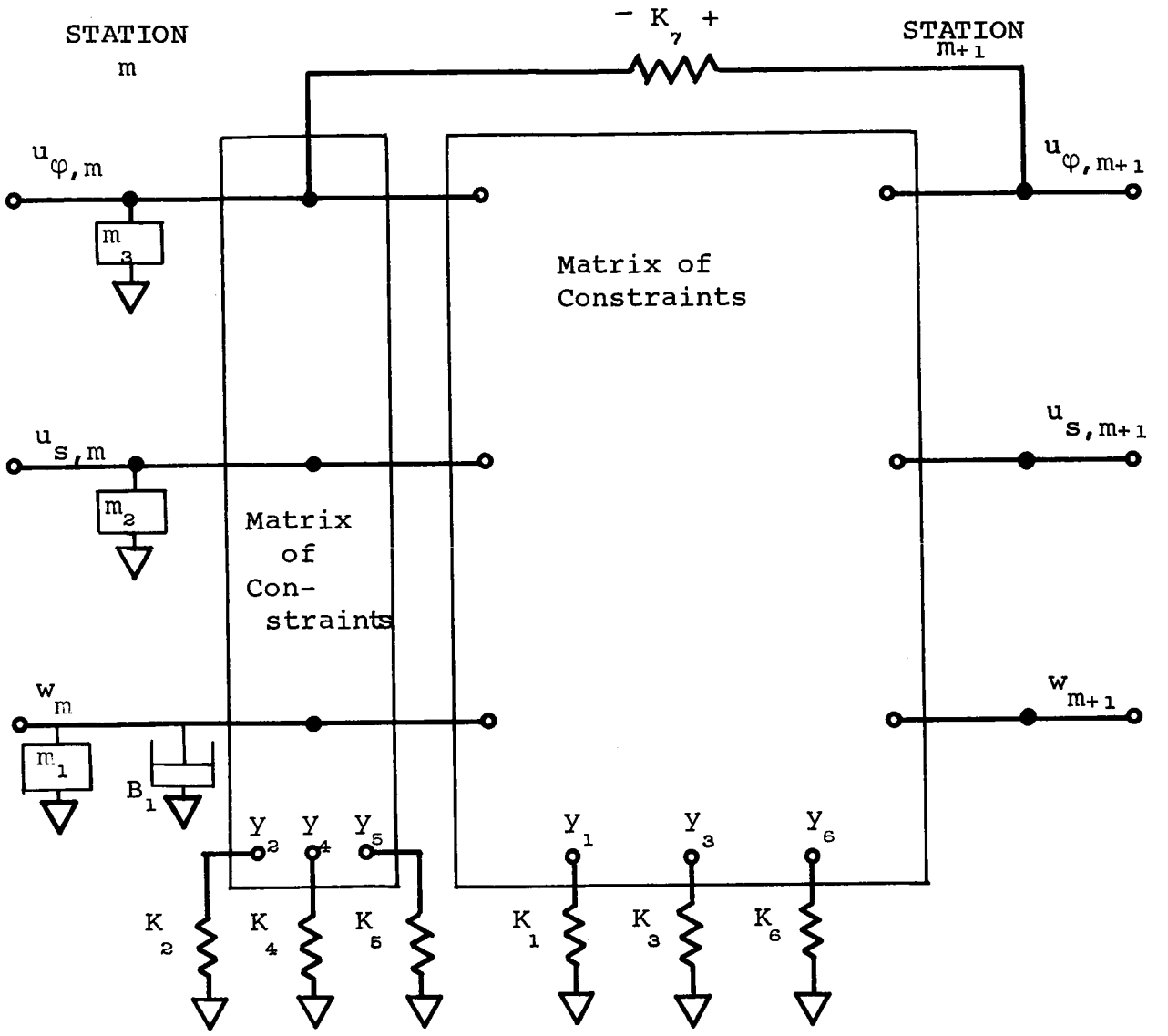

$$y_1 = \epsilon_s + \nu\sqrt{\frac{E_{\varphi\varphi}}{E_{ss}}}\cdot\epsilon_\varphi$$

$$y_2 = \epsilon_\varphi$$

$$y_3 = \epsilon_{s\varphi}$$

$$y_4 = \theta_s$$

$$y_5 = \frac{1}{r}\left[u_s + u_\varphi \cos\beta\right]$$

$$y_6 = -\theta_\varphi$$

Figure 5. — Module for a Section of Membrane Shell

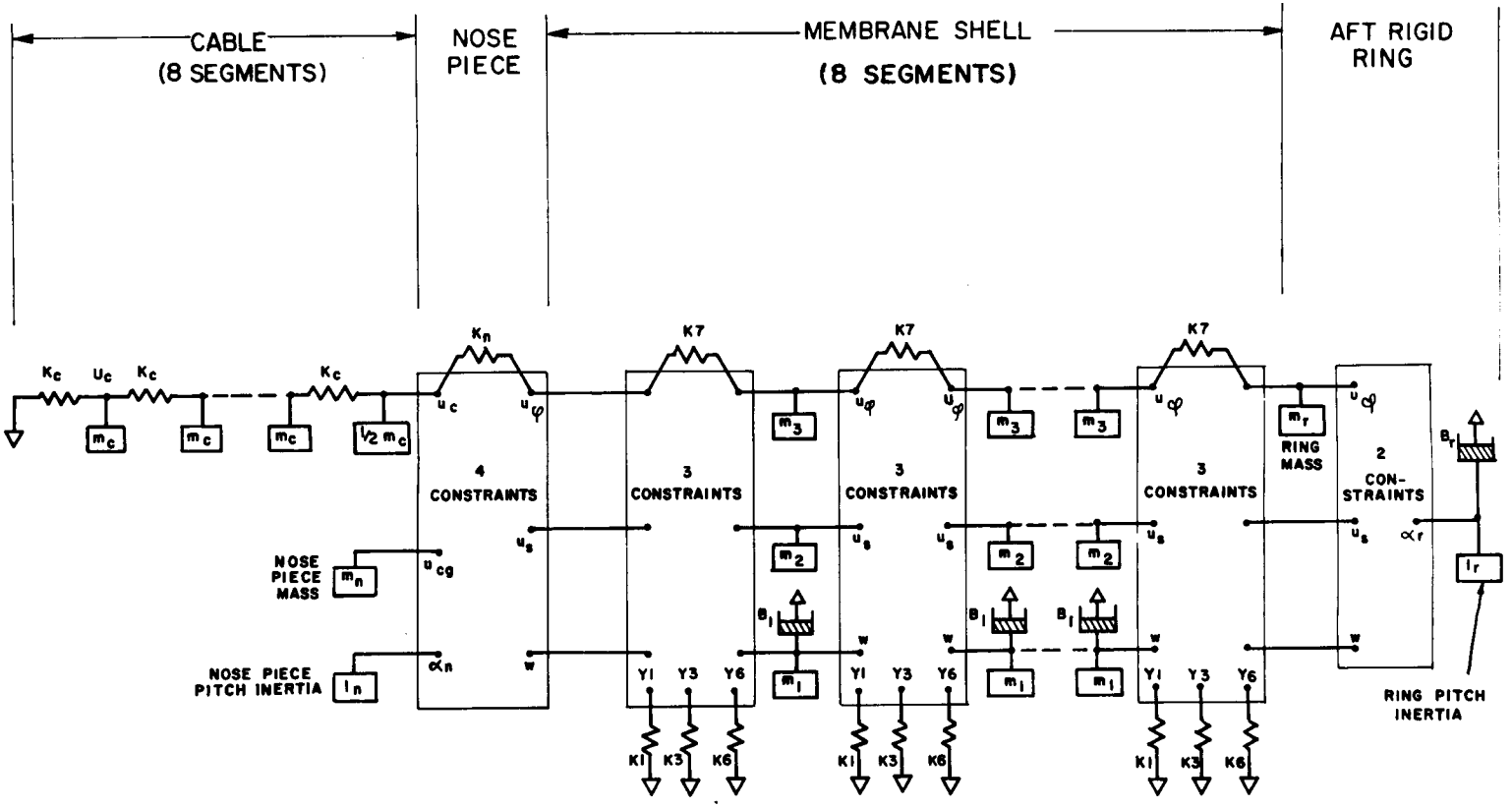

Figure 6. — Lumped Element Model For Complete System

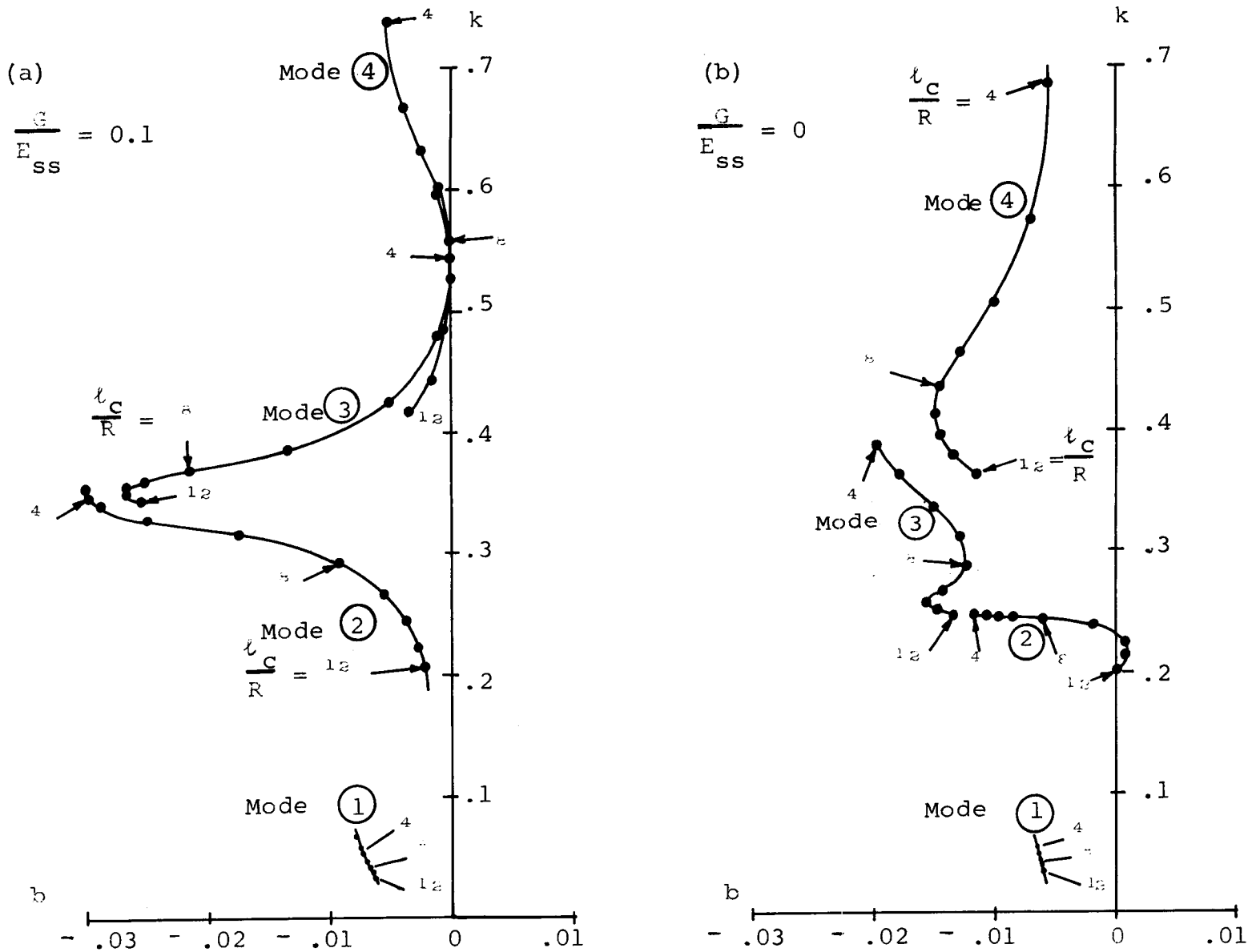

Figure 7. — Root Locus Plots of Flutter Results

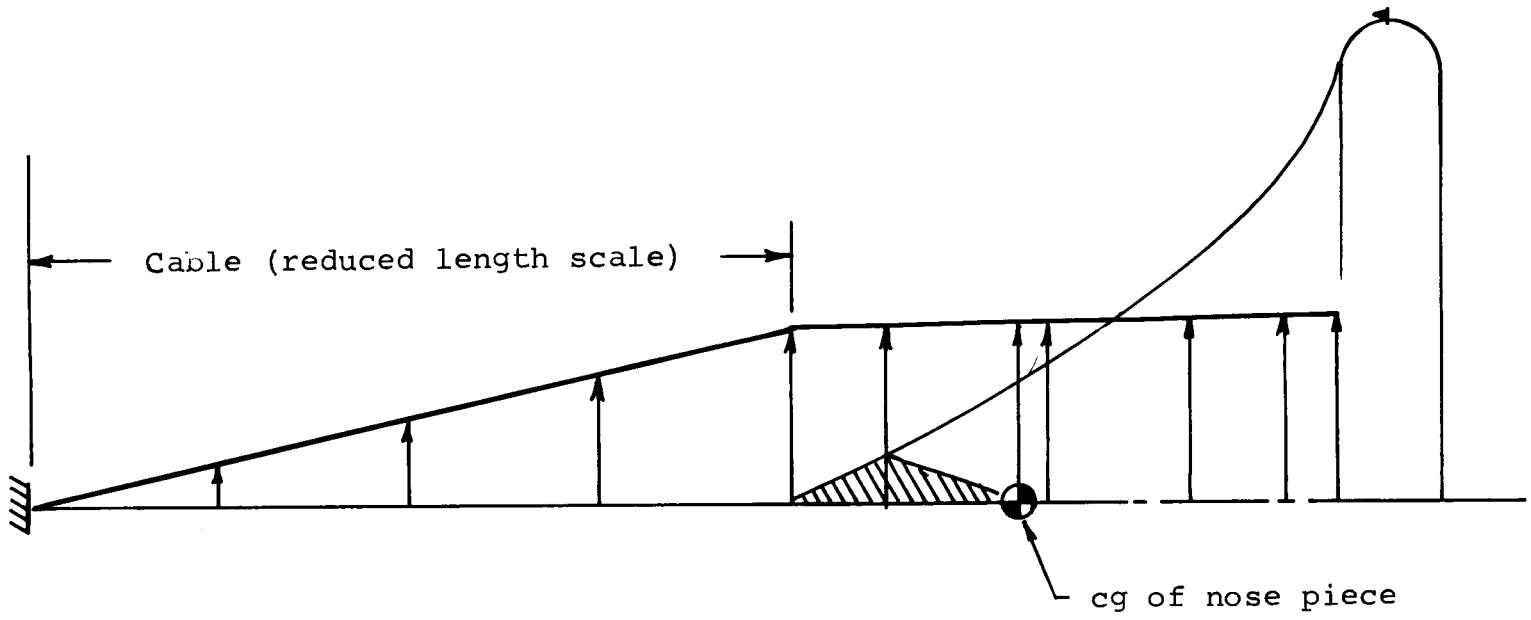

Figure 8. — Mode Shape For First Mode

$$\bar{\ell} = 6$$

$$\frac{G}{E_{ss}} = 0.1$$

$$\frac{\omega R}{V} = .0498 \text{ (1st mode)}$$

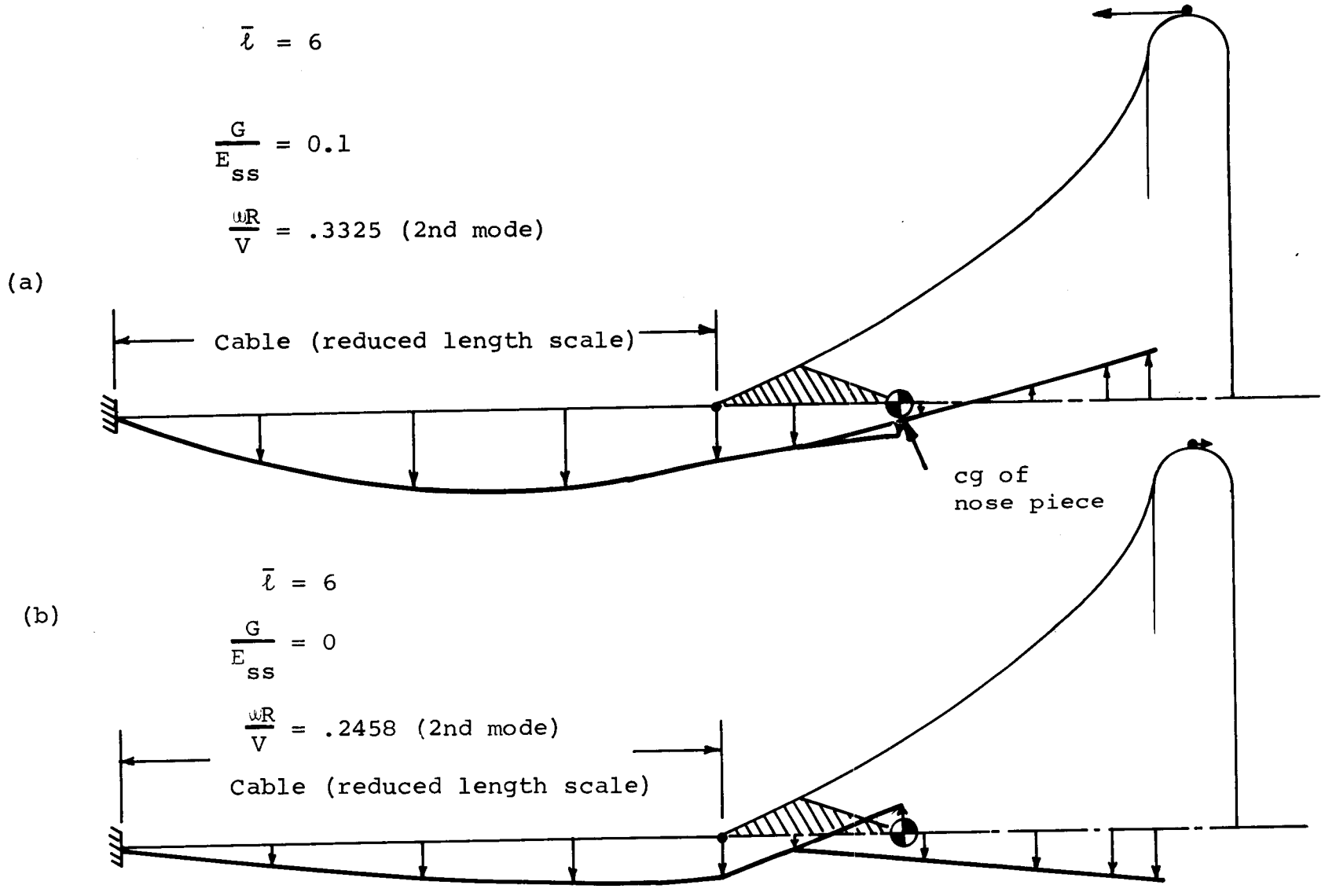

Figure 9. — Mode Shape For 2nd Mode

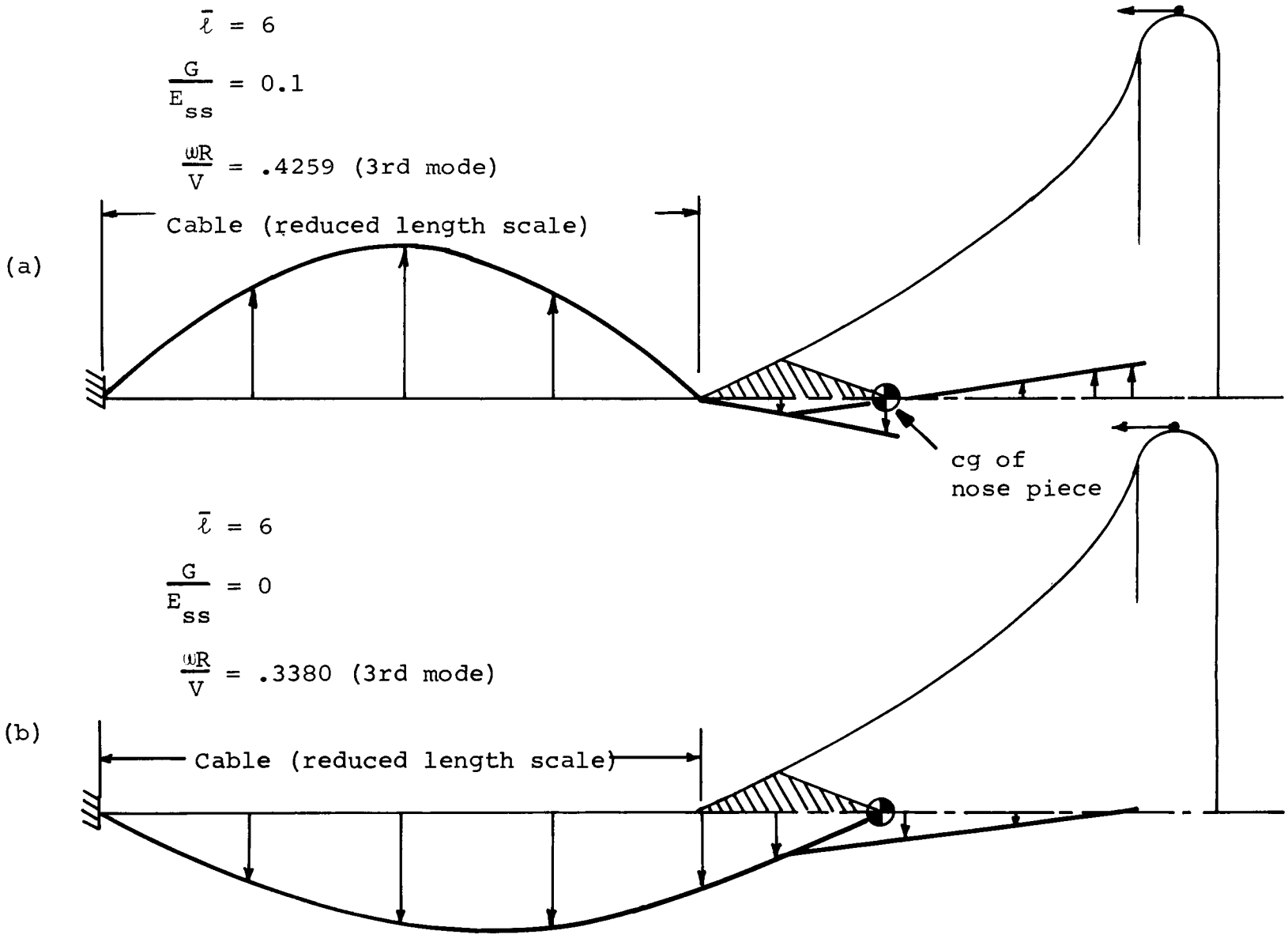

Figure 10. — Mode Shape For 3rd Mode

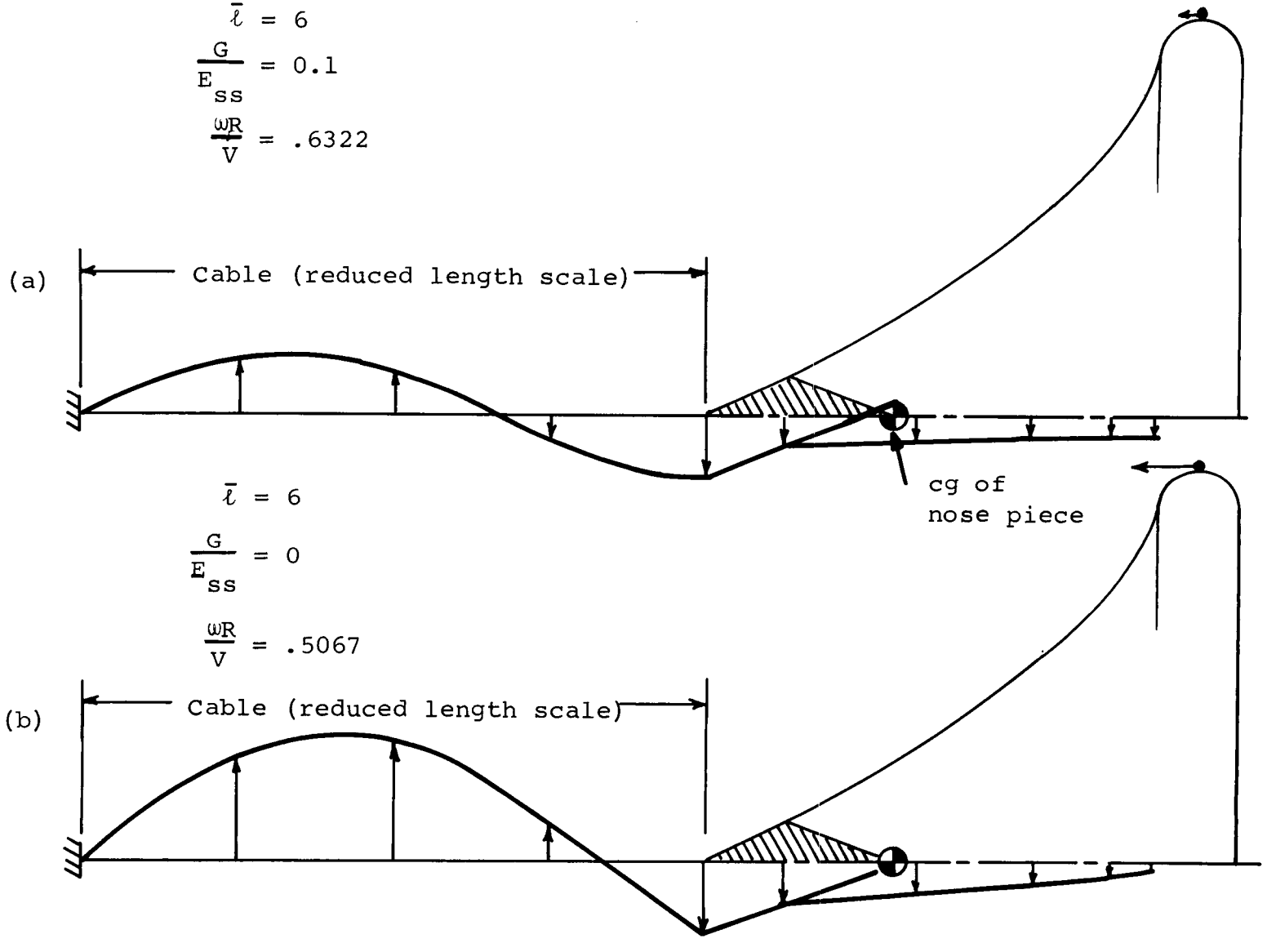

Figure 11. — Mode Shape For 4th Mode

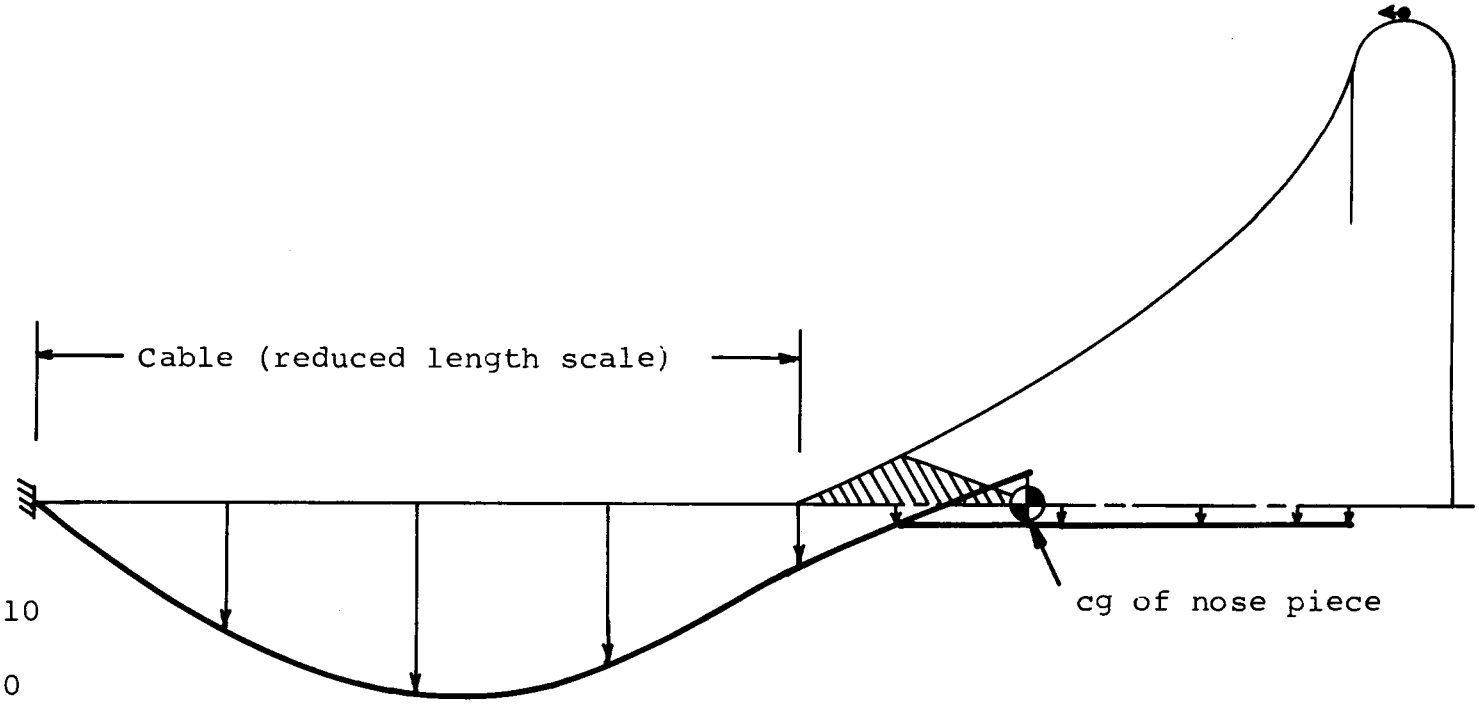

Figure 12. — Flutter Mode

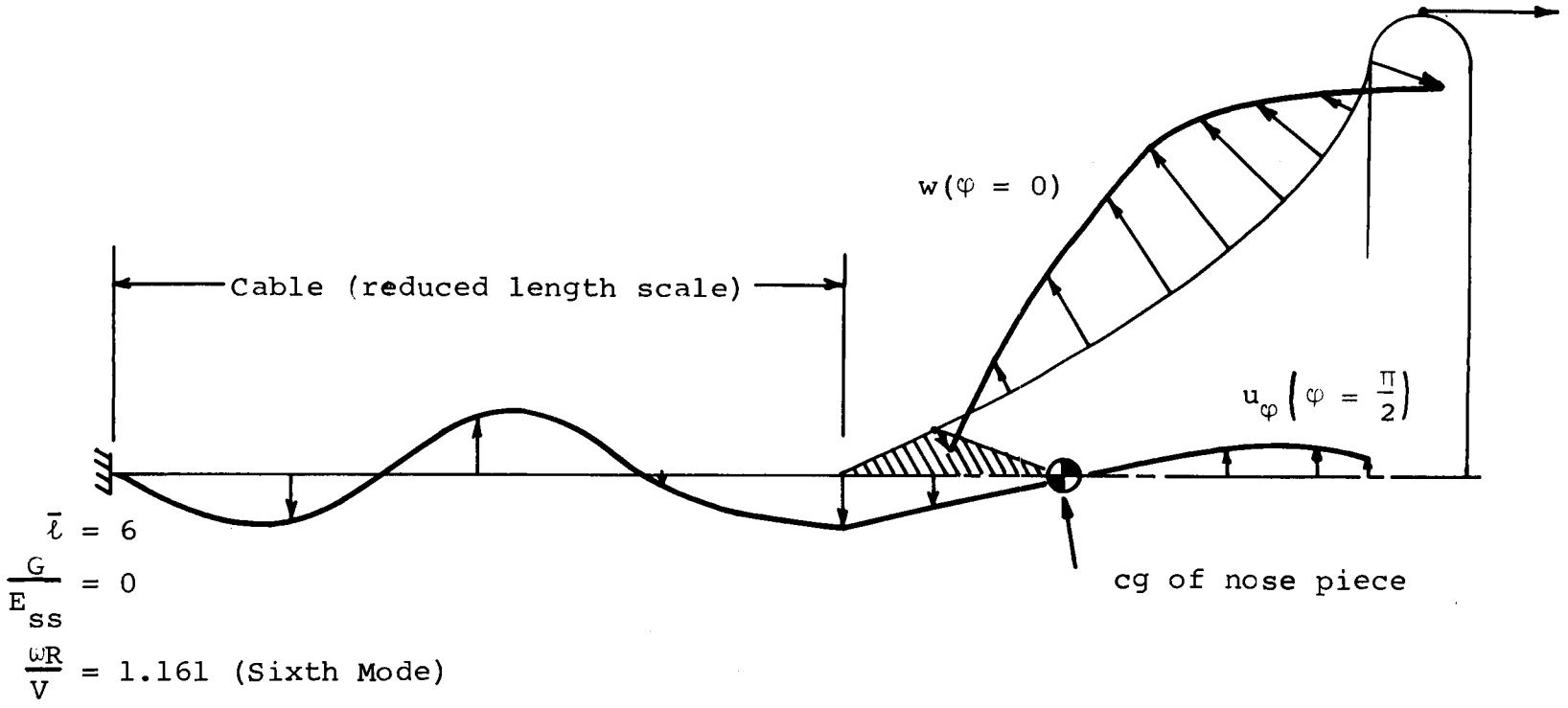

Figure 13. — Mode Shape For Sixth Mode